RSC Advances

PAPER

View Article Online
View Journal | View Issue

Cite this: *RSC Adv.*, 2025, **15**, 8111

Fe_3O_4@SiO_2–BD–DADB-COF is proposed as a novel magnetic covalent organic framework for the determination and extraction of 15 macrolide antibiotics in water and honey†

Hao Zhang,[a] Weihao Ma,[bc] Chunyu Qiang,[a] Jiayuan Nie,[bc] Ling Ma,*[bc] Yawei Zhang*[bc] and Ke Wang *[abc]

Received 5th January 2025
Accepted 26th February 2025

DOI: 10.1039/d5ra00080g

rsc.li/rsc-advances

In our research, an emerging magnetic covalent organic framework (Fe_3O_4@SiO_2–BD–DADB-COF) was formulated through Fourier transform infrared spectroscopy (FT-IR), scanning electron microscopy (SEM), *etc.* Several parameters affecting the extraction process were refined. Accordingly, a novel method of determining 15 macrolides (MALs) in honey and water was established through the Fe_3O_4@SiO_2–BD–DADB-COF as a magnetic solid-phase extraction (MSPE) adsorbent and ultra-performance liquid chromatography-tandem mass spectrometry (UPLC-MS/MS). In consequence, the standard curves for the 15 MALs exhibited an exceptional linearity from 0.1 to 200 μg L^{-1}, and the correlation coefficients (R^2) varied from 0.9990 to 0.9999. The recoveries fell between 70.01% and 115.56%, with the relative standard deviations (RSDs) being below 9.93% (n = 5). The detection limits reached 0.001–0.075 μg L^{-1} with the quantification limits being 0.004–0.228 μg L^{-1}. Ultimately, the method was excellently applied to the analysis of MALs in honey and water.

1. Introduction

Macrolides (MALs) are, actually, a category of antibiotics produced by *Streptomyces* bacteria. MALs are characterized by a big lactone ring (12–16 carbon atoms) attached to sugars *via* glycosidic bonds, making them effective in combating various infections.[1] Gram-positive and Gram-negative bacteria are two common classes of bacteria. Gram-positive bacteria often cause diseases such as skin infections, respiratory tract infections and endocarditis, while Gram-negative bacteria may cause urinary system infections, pneumonia, septicemia and gastrointestinal infections. These bacterial infections, if not treated, can cause serious complications and can even be life-threatening. Fortunately, MALs have been widely used to treat infections caused by Gram-positive and Gram-negative bacteria, providing effective options for clinical treatment.[2] Alarmingly, the overuse and inappropriate use of MALs are still common. In addition, humans and animals cannot fully absorb MALs, with 30% to 90% being excreted in their original form through feces and urine. The rate at which MALs are introduced into the environment exceeds their degradation rate.[3–5] When MALs enter the environment, they not only affect the microbial population of water bodies but also induce the generation of drug-resistant bacterial strains. Hence, the threat to the environment rises. Correspondingly, MALs are capable of entering the human body *via* the food chain, resulting in side impacts, like ototoxicity, gastrointestinal issues, nephrotoxicity, and cochlear nerve damage.[6,7] According to the severity of the above situation, some organizations and nations have formulated the maximum residue limits (MRLs) for MALs among some foods. For example, Japan has set the MRLs of tylosin and tilmicosin in milk at 50 μg kg^{-1},[8] the European Union has set the MRLs of tilmicosin in sheep meat at 50 μg kg^{-1}.[9] As specified by the GB 31650.1-2022, China's National Food Safety Standard, the MRLs for kitasamycin, lincomycin, and tilmicosin from chickens reach 100, 75, and 200 μg kg^{-1} separately, whereas those for MALs in other foods and water (*e.g.*, honey) are reported seldomly. With respect to food security supervision and risk evaluation, it is crucial to develop the approaches to investigating the MAL residues in food and water.

Currently, several methods have been developed for detecting MAL residues. These methods include gas chromatography (GC),[10] high-performance liquid chromatography (HPLC),[11] capillary electrophoresis (CE),[12] and liquid chromatography-tandem mass spectrometry (LC-MS/MS).[13,14] As a high-sensitivity and high-selectivity separation and analysis

[a]*College of Chemistry and Materials Science, Hebei Normal University, Shijiazhuang 050023, China. E-mail: wkecdc@163.com*

[b]*Shijiazhuang Center for Disease Control and Prevention, Shijiazhuang 050011, China. E-mail: mamalin001@163.com*

[c]*Shijiazhuang Technology Innovation Center for Chemical Poison Detection and Risk Early Warning, Shijiazhuang 050011, China. E-mail: 2211291167@qq.com*

† Electronic supplementary information (ESI) available. See DOI: https://doi.org/10.1039/d5ra00080g

method, LC-MS/MS is supported by scholars and researchers. As a vital factor in analytic method, sample pretreatment matters equally in safeguarding the credibility and precision of experimental data.[15,16] To guarantee the precision of LC-MS/MS analyses and overall quality, it is important to value and enhance sample pretreatment technologies.[17]

The most commonly employed pretreatment techniques for MALs include accelerated solvent extraction (ASE),[18] liquid–liquid extraction (LLE),[19] solid-phase extraction (SPE),[20] QuEChERS (Quick, Easy, Cheap, Effective, Rugged and Safe)[21] and magnetic solid-phase extraction (MSPE).[22] Wherein, MSPE is outstanding for a pathbreaking innovation in the realm of separation and enrichment in the 21st century. The most absorbing strength of MSPE becomes the swift and effective analyte extraction through an external magnetic field while highly reducing the pretreatment duration of samples, relative to conventional SPE processes.[23] Due to the fact that magnetic materials are gauged by adsorbents and magnetic nanoparticles, developing such novel substances in MSPE becomes a research focus.

The magnetic materials are composed of magnetic nanoparticles and functional adsorbent materials, with the adsorbent typically coated around the surface of the magnetic nanoparticles. Due to their excellent magnetic properties and good dispersion, Fe_3O_4 nanoparticles are commonly used as the magnetic core for the preparation of magnetic materials.[24] Furthermore, the adsorbent materials commonly employed include metal–organic frameworks (MOFs),[25] porous organic polymers (POPs),[26] molecularly imprinted polymers (MIPs),[27] and covalent organic frameworks (COFs).[28] COFs are outstanding for a category of crystalline porous material relative to other adsorbent materials and draw remarkable attention of researchers owing to their adjustable pore size, exceptional physicochemical stability, and high specific surface region.[29] Wherein, the pore size of COFs substances is capable of being regulated in numerous ways, like choosing discrepant categories of surfactants, integrating pore-expanding agents, *etc.* (*e.g.* reaction time, reaction temperature, pH of the reaction solution).[30] To sum up, these fascinating properties enable the use of COFs in many fields, encompassing material adsorption,[31] gas storage,[32] sensors,[33] and photochemical and heterogeneous catalysis.[34] However, the low density of COFs poses challenges for their separation from solutions, thereby limiting their application in the processing of real samples. The combination of COFs and Fe_3O_4 perfectly compensates for this shortcoming, resulting in magnetic COFs that not only possess a high adsorption capacity but also facilitate separation, which resolves the challenges associated with COF recycling, thereby increasing the convenience and efficiency of the operational process.[24] Although magnetic COF materials for the extraction of antibiotics have been developed, few reports are related to magnetic COF materials for the detection of MALs.[35] Currently, the materials for detecting MALs are mainly focused on MOFs and MIPs.[7,36] They have good chemical stability, but the synthesis steps are complicated, and the number of MALs is less than 7. Therefore, the development of magnetic COF materials is very important for the detection of multiple MALs simultaneously.

In this study, we designed and synthesized a novel Fe_3O_4@SiO_2–BD–DADB-COF on the basis of the structure of MALs *via* a simple reaction of Fe_3O_4@SiO_2, 2,2′-bipyridine-5,5′-dicarboxaldehyde, and 1,3,5-tris(4-aminophenyl) benzene. Importantly, the pore volume and size of this Fe_3O_4@SiO_2–BD–DADB-COF were adjusted by the addition of polyethylene–polypropylene glycol (P-123). Subsequently, the synthesized Fe_3O_4@SiO_2–BD–DADB-COF material was further characterized. Actually, our research explored the desorption condition and extraction, encompassing the quantity of adsorbents, the volume of eluent, the extraction time, *etc.* At last, a novel approach was formulated based on MSPE integrated with UPLC-MS/MS. This was confirmed and utilized to construe 15 MALs in honey and water.

2. Experimental

2.1. Reagents and materials

Tianjin Yongda Chemical Reagent Co., Ltd. (China) provided sodium chloride (NaCl), anhydrous ethanol, ferric chloride hexahydrate ($FeCl_3 \cdot 6H_2O$), ethylene glycol (EG), sodium acetate trihydrate ($CH_3COONa \cdot 3H_2O$), 1,4-dioxane, and acetic acid (HAc). Xiya Chemical Technology Co. Ltd (Shandong, China) supplied PEG-4000 polyethylene glycol, whereas Tianjin Kaitong Chemical Reagent Co. Ltd (China) provided a 25% (w/w) ammonia solution. Dikma supplied formic acid and tetraethoxysilane (TEOS). Polyethylene–polypropylene glycol (P-123) was purchased from Sigma-Aldrich. In addition to 2,2′-bipyridine-5,5′-dicarboxaldehyde, sodium chloride (NaCl) was offered by Aladdin Chemistry Co., Ltd. (Shanghai, China). Methanol (MeOH) was offered by Thermo Fisher Co., Ltd. (USA) and acetonitrile (ACN) was supplied by Merck (Darmstadt, Germany). Through a Millipore Milli-Q Gradient Water Purification System (USA), acetic acid, acetonitrile, and acetonitrile were of HPLC grade and all other reagents were of analytical grade, with ultra-pure water formulated and utilized throughout the experiment.

Ivermectin, tylosin tartrate, selamectin, tilmicosin, eprinomectin, avermectin, kitasamycin, azithromycin, doramectin, emamectin, moximycin tylosin and tylosin were obtained from Dr Ehrenstorfer GmbH. Josamycin, midecamycin and tylvalosin were obtained from MedChemExpress. The chemical structures of the 15 MALs are shown in Table S1.† Table S2† lists the purities and CAS registry numbers of the 15 MALs. Including 1 μg mL^{-1} of each of the 15 MALs, a blended stock standard solution were prepared in ACN and preserved in darkness at −20 °C.

2.2. Instrumental and analytical conditions

A Phenomenex Kinetex F5 column with a 100 Å pore size, dimensions of 3.0 mm × 100 mm, and a 2.6 particle in diameter, was employed to separate the MALs. With a mobile phase of 0.1% formic acid in water (phase A) and 3.0 mL of acetonitrile (phase B), a flow velocity of 0.3 mL min^{-1} was achieved. The process of the gradient elution was listed below: (1) 0–2.5 min, 45% B (v/v); (2) 2.5–2.6 min, 45–55% B (v/v); (3) 2.6–7.5 min,

55% B (v/v); (4) 7.5–7.6 min, 55–75% B (v/v); (5) 7.6–10.5 min, 75% B (v/v); (6) 10.5–10.6 min, 75–45% B (v/v); (7) 10.6–14 min, 45% B (v/v). Fig. S1† describes the chromatograms of 15 MALs.

Detection and analysis were implemented using a UPLC-MS/MS instrument (Exion TRILPLE QUAD 5500, AB SCIEX, USA) and electrospray ionization (ESI) was applied to the positive ion mode, with the data gathered in multiple reaction monitoring (MRM) pattern. The mass spectrometry details for 15 MALs are provided in Table S3.†

The prepared materials were characterized through Fourier transform infrared (FT-IR) (Thermo Nicolet Co. Ltd., USA), Brunauer–Emmett–Teller (BET) method (Quantachrome Instruments, USA), a SQUID XL-7 vibrating sample magnetometer (Quantum Design, USA), a D8A X-ray diffractometer (Germany), and scanning electron microscopy (SEM) with an S-4800 instrument (Japan), as well as transmission electron microscopy (TEM) with an FEI Tecnai G2 F20 (USA).

2.3. Preparation of Fe_3O_4@SiO_2–BD–DADB-COF

2.3.1. Synthesis of Fe_3O_4. Reportedly, the nanoparticles of magnetic Fe_3O_4 were compounded.[37] 1.62 g $FeCl_3 \cdot 6H_2O$ distributed in 60 mL ethylene glycol (EG) stirred vigorously at room temperature (RT). Next, 2.0 g PEG-4000 and 7.2 g $CH_3COONa \cdot 3H_2O$ were supplemented to the solution. In addition, agitation lasted for 30 min till the solution was brownish-yellow to impede particle accumulation. Afterwards, the homogeneous yellow solution was delivered meticulously to one autoclave and then heated up to 200 °C for 8 h. Following cooling to RT, the black product with a washing volume of 15 mL every time, was segregated from the solvent through magnets and rinsed thrice with ultrapure water and absolute ethanol. Afterwards, the sample was dehydrated in a vacuum stove for 3 h at 60 °C.

2.3.2. Synthesis of Fe_3O_4@SiO_2. Through the sol–gel method, the nanoparticles of Fe_3O_4@SiO_2 were compounded.[38] Usually, 200 mg Fe_3O_4 were compounded and then distributed within a mix of 40 mL ultrapure water and 160 mL anhydrous ethanol. In order to evenly distribute, the mixture was sonicated for 30 min. Subsequently, 3 mL aqueous ammonia was integrated with the mixture and then sonicated for 5 min. Under the magnetic agitation, 2 mL TEOS was added meticulously drop by drop. Next, the blend continued to react for 1 day at 30 °C to compound Fe_3O_4@SiO_2. Such sample was rinsed some times through 40 mL anhydrous ethanol before 40 mL ultrapure water. Subsequently, this sample was dehydrated in a vacuum for 3 h at 60 °C.

2.3.3. Synthesis of Fe_3O_4@SiO_2–BD–DADB-COF. The Fe_3O_4@SiO_2–BD–DADB-COF was prepared in light of a prior report and enhanced correspondingly.[39] Fe_3O_4@SiO_2 (150 mg) was integrated into 1,4-dioxane (30 mL) and ultrasonically diffusive for 5 min. Subsequently, 1 g of P-123 was added. Next, 1,3,5-tris(4-aminophenyl)benzene (0.1054 g, 0.3 mmol) and 2,2′-bipyridine-5,5′-dicarboxaldehyde (0.0955 g, 0.45 mmol) were integrated into the solvent. In total, 0.5 mL acetic acid (12 mol L^{-1}) was slowly incorporated into the solution and agitated at RT for 2 h. Then, 4.5 mL acetic acid (12 mol L^{-1}) was supplemented gradually and subsequently reacted for 1 day at 80 °C. Finally, the products were rinsed three times using 30 mL of anhydrous ethanol and dehydrated in a vacuum for 4 h at 60 °C.

2.4. Sample preparation

In Shijiazhuang, Hebei Province, twenty surface water samples were gathered from discrepant rivers, Hebei Province. A filter membrane of 0.45 μm was employed to filter the total water samples. Then, such samples were preserved for MSPE within a refrigerator at 4 °C.

Fifteen honey samples were offered by different supermarkets. Prior to MSPE analysis, 1 g honey sample was delivered to a polypropylene tube of 50 mL in volume. The sample was diluted using 1 mL of ultrapure water. 12 mL acetonitrile was incorporated into the mixture. Next, such solution was sensitive to ultrasonication for 2 min. Subsequently, the tube was centrifuged at 8000 rpm for 5 min. The extract (6 mL) was dehydrated at 35 °C under flowing nitrogen. The residue was lysed in 10 mL ultrapure water again. Afterwards, the mix was vortexed and sonicated. The pH of the mix sample was modulated to 8.

2.5. Procedure of MSPE

Fig. 1 displays the MSPE process. Firstly, 10 mg Fe_3O_4@SiO_2–BD–DADB-COF was added to a 10 mL of sample mixture that was then shaken for 10 min for adsorption. Secondly, an external magnetic field was used to gather the sorbent, with the supernatant abandoned. Thirdly, 8 mL 0.3% ammoniated ACN was supplemented to the sorbent collected, which was then vortexed for 10 min to elute the MALs. Fourthly, the eluent was isolated with a magnet and dehydrated at 35 °C under N_2. Ultimately, the residues were lysed through a 1.0 mL mobile phase again and then filtrated *via* a 0.20 μm membrane. Such residues were injected into the UPLC-MS/MS mechanism for our analysis.

3. Results and discussions

3.1. Characterization of the Fe_3O_4@SiO_2–BD–DADB-COF

The forms of the prepared Fe_3O_4@SiO_2–BD–DADB-COF and Fe_3O_4 materials were characterized *via* TEM and SEM. Fig. 2A exhibits that the Fe_3O_4 nanoparticles are nearly spherical and well dispersed, whereas the SEM image of Fe_3O_4@SiO_2–BD–DADB-COF (Fig. 2B) reveals a relatively rough surface. Further, as described Fig. 2D, the TEM images exhibits the typical core–shell composition of Fe_3O_4@SiO_2–BD–DADB-COF, implying that the COF was stained on the surface of Fe_3O_4 nanoparticles.

Moreover, energy dispersive X-ray (EDS) analysis was conducted, in an attempt to validate the elemental composition of the Fe_3O_4@SiO_2–BD–DADB-COF material. Fig. S2† shows the observed distributions of C, N, O, Si, and Fe, with contents of 63.91%, 8.94%, 17.35%, 1.94% and 7.86%, separately. Specifically, the atomic content of N was 8.94% in Fe_3O_4@SiO_2–BD–DADB-COF, suggesting the excellent synthesis of the COF layer on the Fe_3O_4 surface.

Further, Fig. 3A shows the FT-IR spectra of Fe_3O_4@SiO_2–BD–DADB-COF, Fe_3O_4 and Fe_3O_4@SiO_2. Within the spectra, the

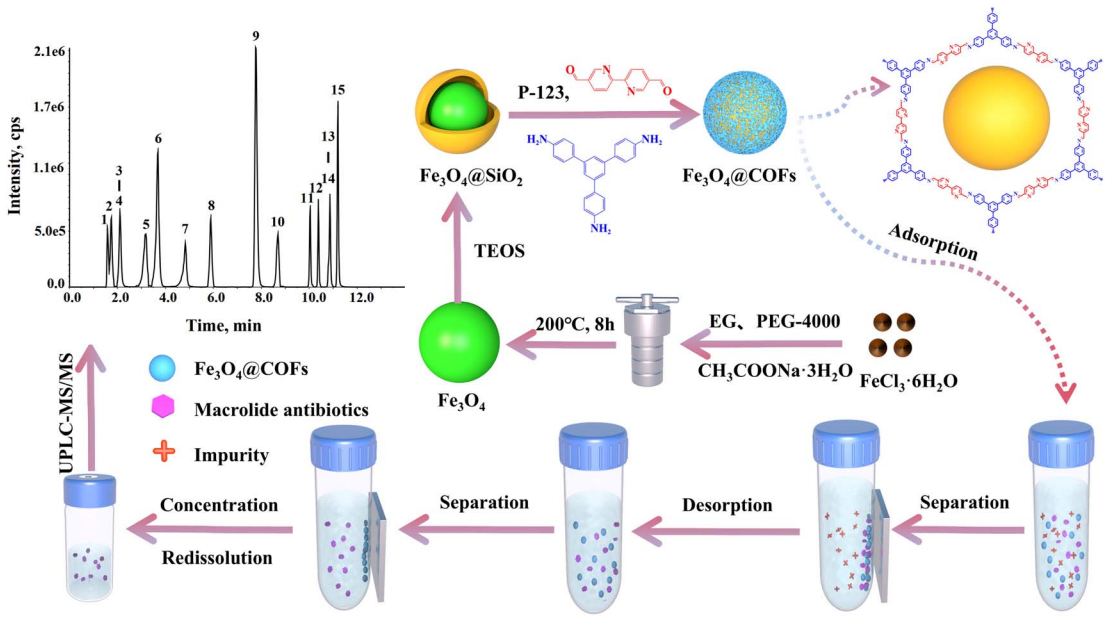

Fig. 1 Scheme illustration for preparation of Fe_3O_4@SiO_2–BD–DADB and the MSPE procedure.

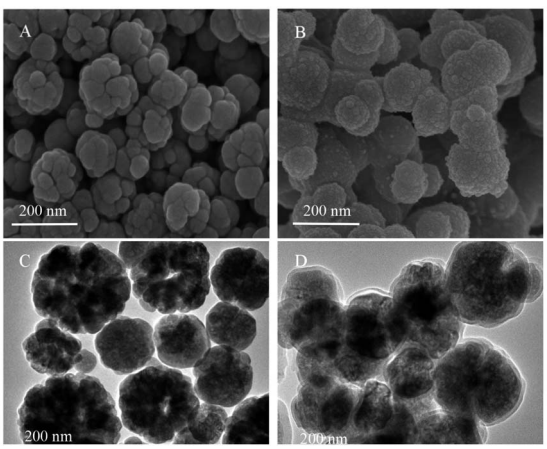

Fig. 2 The SEM of (A) Fe_3O_4, (B) Fe_3O_4@SiO_2–BD–DADB-COF; the TEM of (C) Fe_3O_4, (D) Fe_3O_4@SiO_2–BD–DADB-COF.

absorption peaks at 580 cm^{-1} and 1094 cm^{-1} was consistent with the oscillation of the Fe–O–Fe and Si–O–Si bonds, separately. Consequently, it was validated that the smooth encapsulation of silicon shells emerged on the Fe_3O_4 surface.[40] In addition, the two characteristic peaks at 1586 cm^{-1} and 1495 cm^{-1} were ascribed to the stretching vibrations of the C–N and C–C ring bonds, respectively.[41] Thereby, BD–DADB-COF was grafted on the Fe_3O_4@SiO_2 surface excellently.

What's more, Fig. 3B exhibited that the crystalline structures of Fe_3O_4, Fe_3O_4@SiO_2, and Fe_3O_4@SiO_2–BD–DADB-COF were construed by means of XRD patterns. Fe_3O_4@SiO_2–BD–DADB-COF has characteristic peaks at 30.35°, 35.74°, 43.29°, 53.69°, 57.14°, and 62.77°, aligning with the surface of Fe_3O_4 crystallographic structure (220), (311), (400), (422), (511), and (440), respectively.[42] Furthermore, the Fe_3O_4@SiO_2–BD–DADB-COF exhibited inconspicuous broad characteristic peaks at 23.5°, attributing to π–π stacking.[43] The data illustrated that Fe_3O_4@SiO_2–BD–DADB-COF became exceedingly crystalline and still kept high crystallinity after staining.

Fig. 3C reveals that the porous structure was evaluated through N_2 adsorption determination at 77 K. Fe_3O_4@SiO_2–BD–DADB-COF showed characteristic type IV isotherms. This illustrated its distinctive mesoporous structure.[44] In addition, the BET surface of Fe_3O_4 reached 7.98 $m^2\ g^{-1}$ and came short of the 33.71 $m^2\ g^{-1}$ surface of Fe_3O_4@SiO_2–BD–DADB-COF. Due to increased specific surface area of Fe_3O_4@SiO_2–BD–DADB-COF, more adsorption sites were thus accessible to MALs. In consequence, it indicated that Fe_3O_4@SiO_2–BD–DADB-COF became appropriate as an adsorbent of the MSPE.

The properties of Fe_3O_4 and Fe_3O_4@SiO_2–BD–DADB-COF were measured *via* a vibrating sample magnetometer (VSM). Fig. 3D displays that the saturation magnetization of Fe_3O_4 reaches 79.12 emu g^{-1}, while Fe_3O_4@SiO_2–BD–DADB-COF presented a lower value of 37.02 emu g^{-1}. This decrease was ascribed to the formation of the core–shell in Fe_3O_4@SiO_2–BD–DADB-COF.[45] Despite the decrease in magnetization, Fe_3O_4@SiO_2–BD–DADB-COF still exhibited a magnetic response that was adequate for practical magnetic separation applications. The Fe_3O_4@SiO_2–BD–DADB-COF can be rapidly separated from the solution within 60 seconds *via* an external magnetic field.[46] As depicted in Fig. S3,† a homogeneous dispersion of Fe_3O_4@SiO_2–BD–DADB-COF in water was obtained after ultrasonication, and could be aggregated together by an external magnetic field.

3.2. Condition of MSPE

We optimized the adsorbent dosage, the concentration of salts, the pH of samples, eluate type, eluate volume, elution time, and

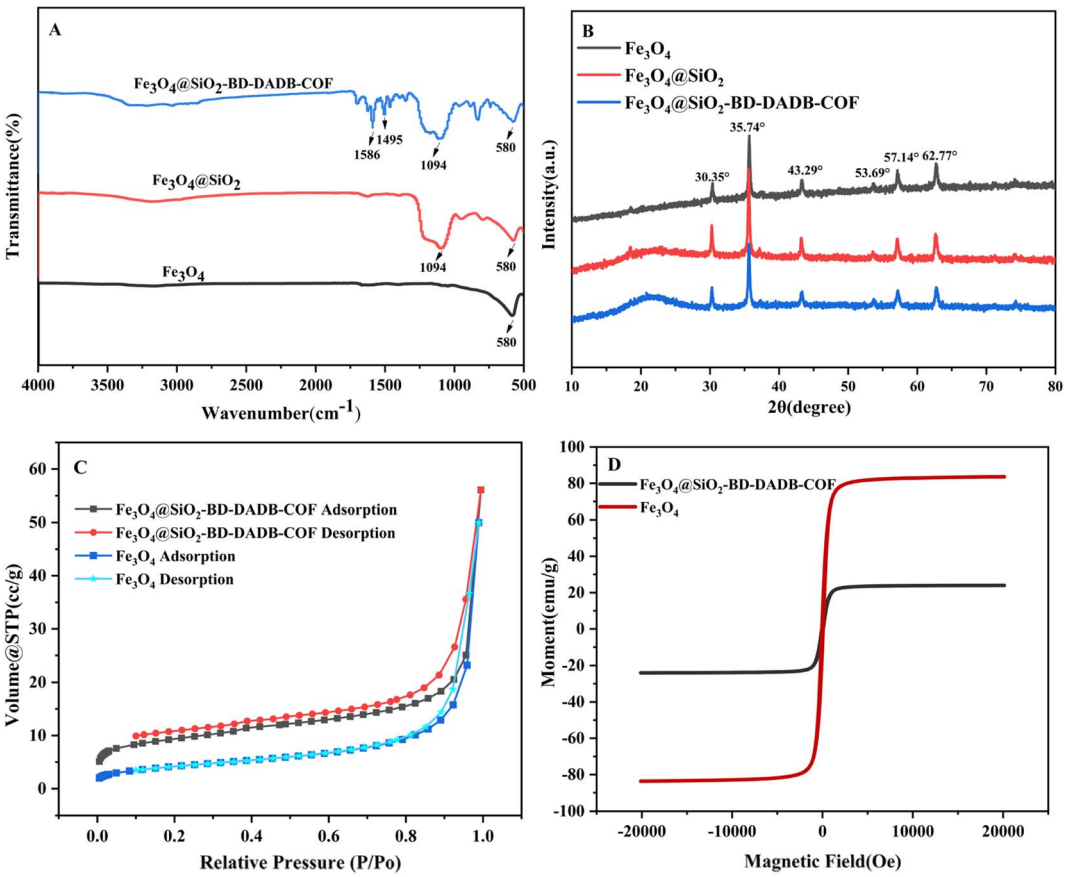

Fig. 3 (A) FT-IR spectra of Fe_3O_4, Fe_3O_4@SiO_2 and Fe_3O_4@SiO_2–BD–DADB-COF; (B) XRD patterns of Fe_3O_4, Fe_3O_4@SiO_2 and Fe_3O_4@SiO_2–BD–DADB-COF; (C) N_2 adsorption–desorption isotherms of Fe_3O_4 and Fe_3O_4@SiO_2–BD–DADB-COF; (D) VSM curves of Fe_3O_4 and Fe_3O_4@SiO_2–BD–DADB-COF.

extraction time to improve the MAL extraction efficiency (EE). Such parameters were systemically explored through a single-factor trial.

3.2.1. Effect of adsorbent dosage. A range of 6–14 mg was carefully examined for various dosages of Fe_3O_4@SiO_2–BD–DADB-COF. Fig. 4A reveals that the EE of MALs gradually rises as the adsorbent dose varies between 6 and 10 mg. However, the recovery of the MALs was still had almost no change at 75.61–105.81% when the dosage surpassed 10 mg, which denoted that an equilibrium was created with Fe_3O_4@SiO_2–BD–DADB-COF at 10 mg. Thereby, 10 mg was applied to follow-up experiments.

3.2.2. Effect of sample solution pH. The pH of the solution sample exerted a substantial impact on the adsorption, because it could alter the molecular morphologies of analytes and the surface variation of the sorbents, thus influencing the EE of the analytes.[47] The pH of the solution sample was set to 3, 5, 7, 8, 9, and 10 to rate the impact of pH. Fig. 4B shows that the maximal recoveries (71.64–105.59%) occurs at pH 8 and then gently declined as the pH varied between 8 and 10. In addition, the zeta potential of Fe_3O_4@SiO_2–BD–DADB-COF was measured across the pH from 3 to 10.[48] Fig. S4† show that the point of zero charge (PZC) of the Fe_3O_4@SiO_2–BD–DADB-COF substance is approximately pH 4.73. Below this pH, the material surface was positively charged; above pH 4.73, it was negatively charged. As the pH was nearly 8, owing to the negative charge on the Fe_3O_4@SiO_2–BD–DADB-COF surface, the electron cloud density of the material rose, which increased the number of hydrogen bonding interactions between the Fe_3O_4@SiO_2–BD–DADB-COF and the MALs.[49] In addition, with the pH being over 8, the hydroxyl groups in the MALs triggered to break hydrogen bonds and then weakened the adsorbent binding for the MALs.[50] Hence, the pH of 8 was regarded as the optimum pH of the sample solution.

3.2.3. Effect of salt concentration. Maybe, the salt concentration impacted the extraction efficiency of MALs with regard to MSPE. For one thing, the viscosity and density of the solution sample increased due to adding salt, which rendered it less beneficial for adsorption. For another, the ionic strength of the solution increased due to adding salt. This reduced the analyte solubility and contributed to adsorption.[51] To explore the impact of the added salt on adsorption and gauge the optimum extraction effectiveness, diverse concentrations of NaCl solution were tested between 0% and 20% (w/v). Fig. 4C shows that the recovery of MALs did not remarkably vary as the NaCl concentration ranged between 0% and 10% (w/v). Except selamectin and tilmicosin, the recovery of MALs progressively declined as the NaCl concentration was more than 10% (w/v). Therefore, follow-up trials were implemented without adding the NaCl.

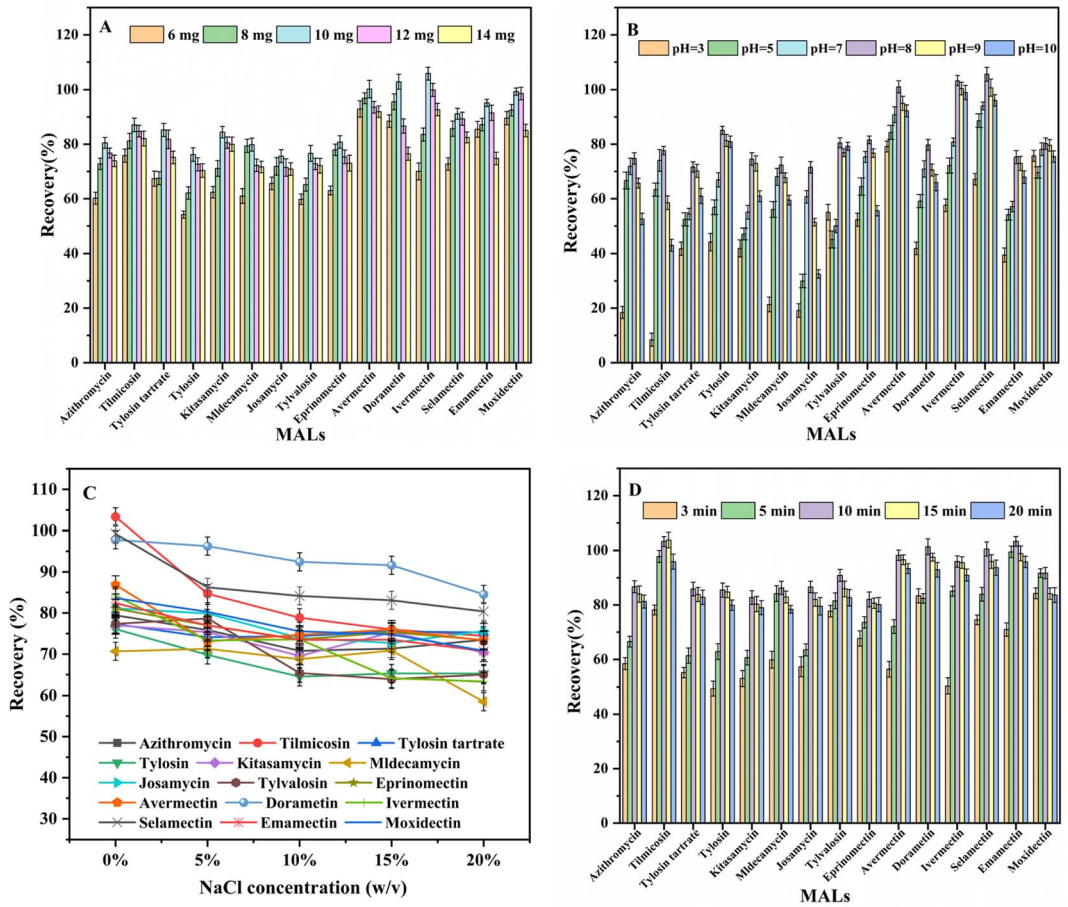

Fig. 4 Effect of (A) adsorbent dosage; (B) sample solution pH; (C) NaCl concentration; (D) extraction time.

3.2.4. Effect of extraction time. The distribution equilibrium of MSPE between the adsorbent and the sample mixture was examined,[52] with an emphasis on investigating the influence of extraction time on the EE from 3 to 20 min. As indicated in Fig. 4D, from 3 to 10 min, the overall recoveries of the MALs tended to increased. When the extraction time was deeply prolonged to 20 min, no remarkable improvement emerged in extraction efficiency. Therefore, such extraction time was gauged to reach 10 min.

3.2.5. Investigation of desorption parameters. The elution solvent type becomes a crucial factor in the MSPE process. Discrepant categories of organic solvents, like ACN, MeOH, ammoniated ACN, and acidified ACN, were chosen as elution solvents with the intention of eluting the adsorbed MALs. Fig. 5A shows that ACN proves a significantly higher elution efficiency than MeOH. However, when ACN was utilized as the elution solvent, the holistic recoveries came short of 85%. The alkaline substances contained in ACN facilitated the elution of MALs.[53] Therefore, further research was conducted to investigate different concentrations of ammonia in ACN. The desorption efficiency gradually increased as the ammonia concentration in ACN increased, with the highest recovery of MALs achieved when 0.3% ammoniated acetonitrile was used as the elution solvent. When the ammonia concentration in ACN increased, the recoveries did not change significantly. Thus, 0.3% ACN ammoniated was utilized as the eluent.

Moreover, the volume of elution solvent (0.3% ammoniated ACN) was analysed. Fig. 5B shows the related results. 8 mL elution solvent was adequate to obtain the excellent desorption efficiencies of the MALs. The recoveries declined mildly with the eluent volume increasing in depth. Therefore, 8 mL was chosen as the elution volume.

Additionally, the desorption time, which was explored within the scope of 6 to 14 min, also impacted the extraction efficiency. The results (Fig. 5C) reveals that the maximal recoveries of MALs were fulfilled at 12 min (71.76–102.13%), no remarkable variations occurred with the prolonged desorption times. As a result, a desorption time of 12 min was chosen for our research.

3.3. Adsorption mechanism

The adsorption systems of Fe_3O_4@SiO_2–BD–DADB-COF towards MALs were investigated in detail. First, the MALs extraction efficiencies of Fe_3O_4@SiO_2 and Fe_3O_4@SiO_2–BD–DADB-COF were compared. Fig. S5† shows that the adsorption of the prepared Fe_3O_4@SiO_2–BD–DADB-COF adsorbent for MALs exceeded that of Fe_3O_4@SiO_2, suggesting that BD–DADB-COF showed outstanding adsorption volume for MALs.

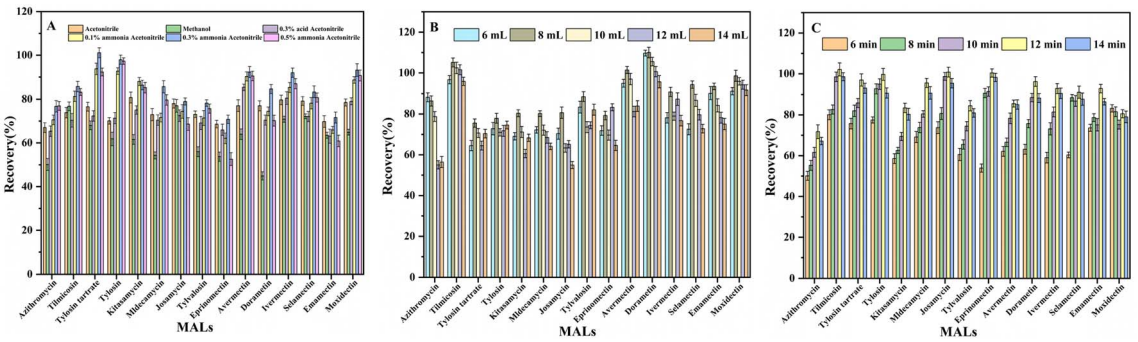

Fig. 5 Effect of (A) elution solvents; (B) elution volume; (C) desorption time.

Furthermore, The C=O and C=C bonds in MALs could form π–π interactions with the large π-conjugation system in the Fe_3O_4@SiO_2–BD–DADB-COF, thereby contributing to the increase in the adsorption effect.[54] The H atoms on the hydroxyl groups in MALs could form hydrogen bonds with the electronegative N atoms in Fe_3O_4@SiO_2–BD–DADB-COF, improving the adsorption efficiency of the material.[55]

Furthermore, as shown in Fig. S4,† when the pH is 8, the negative charge on the Fe_3O_4@SiO_2–BD–DADB-COF surface led to an increase in the electron cloud density of the material. This further facilitated the formation of hydrogen bonds between the Fe_3O_4@SiO_2–BD–DADB-COF and the H atoms of the hydroxyl groups in MALs. Additionally, through zeta potential analysis, the Fe_3O_4@SiO_2–BD–DADB-COF carries a negative charge under conditions of pH 8. The MALs contain amino structures, These amino groups are prone to protonation. Under neutral to weak alkaline conditions, the positively charged MALs (pK_a = 7–9.5) interact with the negatively charged Fe_3O_4@SiO_2–BD–DADB-COF through electrostatic attraction.[56] Moreover, the hydrophobicity affected the adsorption efficiency. The hydrophilicity and hydrophobicity were closely related to the magnitude of the log P value, and the dividing line between hydrophobicity and hydrophilicity was generally considered 1 (greater log P values indicated greater hydrophobicity).[57] As hydrophobic compounds, MALs are characteristic of a macrocyclic lactone ring (log P > 1),[58,59] with the Fe_3O_4@SiO_2–BD–DADB-COF surface encompassing numerous benzene rings. This contributes to adsorbing the MALs *via* hydrophobic effects.[60] In consequence, the dominant adsorption systems of MALs and Fe_3O_4@SiO_2–BD–DADB-COF were regarded as π–π interactions, hydrophobic interactions, *etc.*

Furthermore, the specific surface area of Fe_3O_4@SiO_2–BD–DADB-COF without the addition of P-123 in the synthesis of magnetic COF materials was 12.46 $m^2\ g^{-1}$. However, a larger specific surface area (33.71 $m^2\ g^{-1}$) was obtained by adding P-123 in the synthesis, which could offer more contact sites while improving the adsorption volume of the magnetic COF materials. Fig. S6† displays that when the Fe_3O_4@SiO_2–BD–DADB-COF was prepared, adding P-123 as a pore-expanding agent enhanced recoveries of MALs, increasing them from 48.31–94.34% to 78.23–109.32%. The results indicated that the addition of P-123 during the synthesis of Fe_3O_4@SiO_2–BD–DADB-COF improved the material's adsorption efficiency. To deeply investigate the adsorption selectivity of Fe_3O_4@SiO_2–BD–DADB-COF for MALs, three categories of antibiotics, namely, quinolones (QNs), sulfonamides (SAs), and nitroimidazoles (NDZs), were selected for evaluating selectivity. Table S4† exhibits that the adsorption capacity for MALs varied between 82.92 and 109.54%, whereas the adsorption efficiency of all other antibiotics was below 30%. This may primarily be attributed to electrostatic interactions. Based on zeta potential analysis, Fe_3O_4@SiO_2–BD–DADB-COF is negatively charged at pH 8. QNs (pK_a = 5.2–6.6), SAs (pK_a = 6–7.5), and NDZs (pK_a = 3–6) are negatively charged at pH 8, resulting in electrostatic repulsion with the negatively charged Fe_3O_4@SiO_2–BD–DADB-COF, which hinders their adsorption. In contrast, MALs carry a positive charge at pH 8 and interact with the negatively charged Fe_3O_4@SiO_2–BD–DADB-COF through electrostatic interactions, thereby promoting the adsorption of MALs by Fe_3O_4@SiO_2–BD–DADB-COF. The above results further revealed that Fe_3O_4@SiO_2–BD–DADB-COF was capable of showing the selectivity to MALs.

In Fig. 3C, the N_2 adsorption–desorption isotherms of Fe_3O_4@SiO_2–BD–DADB-COF exhibited nearly overlapping curves within the relative pressure range of $0.1 < P/P_0 < 0.65$, accompanied by an upward trend, indicating simultaneous single and multi-layer adsorption in this region. As the relative pressure (P/P_0) increased to 0.65–0.95, hysteresis in the desorption isotherm was observed, attributed to capillary condensation. The results demonstrate that the Fe_3O_4@SiO_2–BD–DADB-COF functions through a combination of single-layer and multi-layer adsorption mechanisms.[61,62] In addition, the adsorption capacity of the Fe_3O_4@SiO_2–BD–DADB-COF for MALs was investigated by measuring a set of spiked water samples with different concentration, and the capacity of the adsorbent was 678 μg g^{-1}, which displayed good adsorption ability.

3.4. Reusability of the adsorbent

The performance of adsorbents can be evaluated by considering their reusability as a key factor. With adsorption and desorption achieved, the Fe_3O_4@SiO_2–BD–DADB-COF was rinsed using 0.3% ammonia ACN three times, and dehydrated for 4 h in a vacuum at 60 °C, followed by use. Fig. S7† shows that the adsorbent is adopted four times with no prominent decline in the recovery of MALs, which still remained greater than 74.11%.

Consequently, it indicated that the Fe_3O_4@SiO_2–BD–DADB-COF was an adsorbent with outstanding reusability.

3.5. Matrix effect

Given that the intricate matrices among samples affected the precision of the analysis results, the matrix effects (MEs) were examined. The formula of ME is listed below:[63]

$$\mathrm{ME}(\%) = \frac{\text{slope of calibration curve in matrix}}{\text{slope of calibration curve in solvent}} \times 100$$

Providing that the matrix effect (ME) came short of 80.0%, it suggested inhibition; conversely, if the ME exceeded 120.0%, it indicated an enhancement effect. When the ME fell within the range of 80.0% to 120.0%, the matrix effect could be considered negligible. Based on the calculation results in Table S5,† the ME values for the 15 MALs varied between 81.10% and 118.89% in water samples and from 81.57% to 115.66% in honey samples. Consequently, the matrix effect was deemed negligible.

3.6. Method validation

3.6.1. Linearity, LODs, and LOQs. Table 1 lists the analysis performance of the formulated MSPE-UPLC-MS/MS method under the optimum conditions. The scope of 15 MALs was linear, ranging from 0.1–200 μg kg^{-1}, with R^2 values varying between 0.9990 and 0.9999 for water samples. The LOD (S/N = 3) was from 0.001 to 0.075 μg kg^{-1}, with the LOQ (S/N = 10) being from 0.004 to 0.228 μg kg^{-1}. For honey samples, the LODs reached 0.002–0.067 μg kg^{-1}, with the LOQs reaching 0.007–0.202 μg kg^{-1}. Accordingly, it indicated that the method showed the outstanding linearity as well as the escalated sensitivity.

3.6.2. Recovery and precision. Indeed, three discrepant standard concentrations of 15 MALs in honey and water samples were detected. Table S6† shows that 15 MALs experienced exceptional recoveries in honey and water samples, which reached 70.93–115.56% and 70.10–111.73%, respectively. To evaluate the accuracy of this approach, the assay was duplicated multiple times (n = 5). As to the total analytes, the corresponding standard deviation was below 9.78%, proving the credibility of the method.

3.7. Method application in real samples

Our method was employed to construe 15 honey samples and 20 water samples. Azithromycin was explored among two of water samples, showing the concentrations of 0.688 μg L^{-1} and 0.346 μg L^{-1}. Therefore, despite insufficient regulation for MRLs in water, this deserves attention.

3.8. Comparison with other methods

Table 2 summarizes the comparison between the formulated MSPE-UPLC-MS/MS method and other methods to gauge the MALs, including sample matrices, extraction methods, analytical approaches, recoveries, extraction times, and LODs. First, SPE is commonly used pretreatment method for detecting MALs. MSPE eliminates tedious and intricate processes relative to conventional SPE, which simplifies the extraction procedure by separating the sample using an external magnetic field.[6,64,65] Comparison with HLB columns, the synthesized Fe_3O_4@SiO_2–BD–DADB-COF demonstrated a shorter extraction time (10 min), more number of MALs (15), and lower detection limits (0.002–0.067 μg kg^{-1}). Second, each previously reported method has focused on the analysis of a single sample type. In contrast, the method developed in this work has been successfully applied to two distinct sample types.[56] Furthermore, compared with Ol-Fe_3O_4 MNPs and Fe_3O_4@PDA-HPMIPs, the Fe_3O_4@SiO_2–BD–DADB-COF showed significant adsorption capacity and can efficiently adsorb more MALs. Meanwhile, it also exhibits higher recoveries (71.4–105.1%) and lower detection limits (0.001–0.075 μg L^{-1}), showing a high sensitivity of the Fe_3O_4@SiO_2–BD–DADB-COF.[56,64] In consequence, our method

Table 1 Linear range, linear equations, correlation coefficient (R^2), LODs and LOQs of 15 MALs in water and honey

Analytes	Linear range (μg L^{-1})	Linearity equation	R^2	LOD		LOQ	
				Water (μg L^{-1})	Honey (μg kg^{-1})	Water (μg L^{-1})	Honey (μg kg^{-1})
Azithromycin	0.1–200	Y = 11 856.4X + 27 654.4494	0.9990	0.011	0.008	0.037	0.025
Tilmicosin	0.1–200	Y = 2848.2X + 67.91653	0.9995	0.038	0.025	0.114	0.076
Tylosin tartrate	0.1–200	Y = 561 50X + 13 288.68202	0.9999	0.002	0.002	0.009	0.007
Tylosin	0.1–200	Y = 38 568.7X + 3.33625	0.9991	0.011	0.012	0.037	0.036
Kitasamycin	0.1–200	Y = 35 711.4X + 16 478.9553	0.9990	0.010	0.002	0.029	0.007
Midecamycin	0.1–200	Y = 1 219 57X + 183 036	0.9993	0.003	0.004	0.009	0.011
Josamycin	0.1–200	Y = 44 331.8X + 64 300.8	0.9995	0.041	0.002	0.123	0.006
Tylvalosin	0.1–200	Y = 17 234.1X + 482.52347	0.9997	0.030	0.005	0.090	0.014
Eprinomectin	0.1–100	Y = 8768.3X + 15 308.6682	0.9990	0.001	0.064	0.004	0.195
Avermectin	0.1–200	Y = 5465.1X + 1863.66417	0.9993	0.039	0.013	0.119	0.038
Dorametin	0.1–200	Y = 4132.8X + 5.73290	0.9997	0.075	0.060	0.228	0.202
Ivermectin	0.1–200	Y = 6069.4X + 5182.20606	0.9993	0.035	0.004	0.107	0.011
Selamectin	0.1–200	Y = 11 625.2X + 1304.40351	0.9999	0.029	0.036	0.087	0.109
Emamectin	0.1–200	Y = 1 449 93X + 2.29707	0.9991	0.014	0.030	0.042	0.092
Moxidectin	0.1–100	Y = 79 706.9X + 9087.1	0.9998	0.018	0.008	0.014	0.024

Table 2 Comparison of the proposed with other methods for the extraction of MALs

Analysis method	Adsorbent	Matrix (numbers of MALs)	Extraction time (min)	Recovery (%)	LODs	Ref.
MSPE-LC-MS/MS	Ol-Fe_3O_4 MNPs	Water (4)	5	54–117	0.011–0.026 μg L^{-1}	64
SPE-LC-MS/MS	Oasis HLB cartridges	Honey (3)	25	80.94–109.26	0.4–2 μg kg^{-1}	65
SPE-LC-MS/MS	Porous aromatic framework (PAF)	Chicken (6)	50	82.1–101.4	0.2–0.5 μg L^{-1}	6
MSPE-LC-MS/MS	Fe_3O_4@PDA–HPMIPs	Honey (7)	15	84.2–117	0.003–0.076 μg kg^{-1}	56
MSPE-LC-MS/MS	Fe_3O_4@SiO_2–BD–DADB-COF	Water and honey (15)	10	71.4–105.1 75.1–101.9	0.001–0.075 μg L^{-1} 0.002–0.067 μg kg^{-1}	This work

was highly prone to the enrichment and exceedingly sensitive to measure the trace MALs.

4. Conclusions

Through the P-123 as a pore-expanding agent, we successfully synthesized a new covalent organic framework material, Fe_3O_4@SiO_2–BD–DADB-COF, which had several advantages, like exceptional magnetism, reusability, and a high specific surface region. A high-throughput analysis technique was formulated, which integrated the adsorbent with UPLC-MS/MS, to synchronously gauge MALs in water and honey samples. Such an approach was characterized by low detection and quantification limits, a simple extraction procedure, and an exceptional linear range. This lays a good groundwork for supervising MALs in both water and honey.

Data availability

The data that has been used is confidential.

Author contributions

Hao Zhang: conceptualization, methodology, formal analysis, writing – original draft. Weihao Ma: data curation, methodology. Chunyu Qiang: data curation, validation. Jiayuan Nie: methodology, validation. Ling Ma: conceptualization, supervision, funding acquisition. Yawei Zhang: data curation, methodology. Ke Wang: resources, funding acquisition, supervision, data curation, project administration, writing – review & editing. All authors have read and agreed to the published version of the manuscript.

Conflicts of interest

There are no conflicts to declare.

Acknowledgements

This work was supported by the National Natural Science Foundation of China (81903322), the S&T Program of Hebei (223777116D) and the Central Government Guides the Development of Local Science and Technology Project of Hebei Province (246Z7721G).

References

1 R. Cañadas, R. M. G. Martínez, G. P. González and P. F. Hernando, *Polymer*, 2022, **249**, 124843.
2 M. A. García-Mayor, A. Gallego-Picó, R. M. Garcinuño, P. Fernández-Hernando and J. S. Durand-Alegría, *Food Chem.*, 2012, **134**, 553–558.
3 G. El-Saber Batiha, A. Alqahtani, O. B. Ilesanmi, A. A. Saati, A. El-Mleeh, H. F. Hetta and A. M. Beshbishy, *Pharmaceuticals*, 2020, **13**, 196.
4 A. G. Myers and R. B. Clark, *Acc. Chem. Res.*, 2021, **54**, 1635–1645.
5 A. Pani, M. Lauriola, A. Romandini and F. Scaglione, *Int. J. Antimicrob. Agents*, 2020, **56**, 106053.
6 C. Lan, D. Yin, Z. Yang, W. Zhao, Y. Chen, W. Zhang and S. Zhang, *J. Anal. Methods Chem.*, 2019, **2019**, 6849457.
7 Y. Zhou, T. Zhou, H. Jin, T. Jing, B. Song, Y. Zhou, S. Mei and Y. I. Lee, *Talanta*, 2015, **137**, 1–10.
8 G. Lu, Q. Chen, Y. Li, Y. Liu, Y. Zhang, Y. Huang and L. Zhu, *Food Res. Int.*, 2021, **147**, 110450.
9 W. Zhou, Y. Ling, T. Liu, Y. Zhang, J. Li, H. Li, W. Wu, S. Jiang, F. Feng, F. Yuan and F. Zhang, *J. Chromatogr. B: Anal. Technol. Biomed. Life Sci.*, 2017, **1061–1062**, 411–420.
10 Z. Wang, R. C. Beier and J. Shen, *TrAC, Trends Anal. Chem.*, 2017, **92**, 42–61.
11 M. J. G. de la Huebra, G. Bordin and A. R. Rodríguez, *Anal. Chim. Acta*, 2004, **517**, 53–63.
12 A. S. Lorenzetti, A. G. Lista and C. E. Domini, *LWT*, 2019, **113**, 108334.
13 J. V. Grutes, R. G. Ferreira, M. U. Pereira, F. S. Candido and B. F. Spisso, *J. Environ. Sci. Health, Part B*, 2021, **56**, 197–211.
14 V. G. Amelin and D. S. Bol'shakov, *Moscow Univ. Chem. Bull.*, 2019, **74**, 63–69.
15 Q. Zhuang, X. Li, X. Lian, H. Hu, N. Wang, J. Wu, K. Miao, G. Feng and X. Luo, *Cryst. Growth Des.*, 2024, **25**, 319–329.
16 H. Cheng, R. Chen, Y. Zhan, W. Dong, Q. Chen, Y. Wang, P. Zhou, S. Gao, W. Huang, L. Li and J. Feng, *Anal. Chem.*, 2024, **96**, 18555–18563.
17 D. Che, J. Cheng, Z. Ji, S. Zhang, G. Li, Z. Sun and J. You, *TrAC, Trends Anal. Chem.*, 2017, **97**, 1–14.
18 Y. Tao, G. Yu, D. Chen, Y. Pan, Z. Liu, H. Wei, D. Peng, L. Huang, Y. Wang and Z. Yuan, *J. Chromatogr. B: Anal. Technol. Biomed. Life Sci.*, 2012, **897**, 64–71.

19 L. Jank, M. T. Martins, J. B. Arsand, T. M. Campos Motta, R. B. Hoff, F. Barreto and T. M. Pizzolato, *Talanta*, 2015, **144**, 686–695.
20 S. Kheirandish, S. Goudarzi, M. Amirahmadi, S. Ghareghani, H. Ghafari, B. Daraei and M. Ghazi-Khansari, *Microchem. J.*, 2023, **193**, 109103.
21 B. F. d. M. Pereira, M. U. Pereira, R. G. Ferreira and B. F. Spisso, *Food Anal. Methods*, 2020, **14**, 719–733.
22 I. S. Ibarra, J. M. Miranda, J. A. Rodriguez, C. Nebot and A. Cepeda, *Food Chem.*, 2014, **157**, 511–517.
23 V. V. Tolmacheva, V. V. Apyari, A. A. Furletov, S. G. Dmitrienko and Y. A. Zolotov, *Talanta*, 2016, **152**, 203–210.
24 L. You, K. Xu, G. Ding, X. Shi, J. Li, S. Wang and J. Wang, *J. Mol. Liq.*, 2020, **320**, 114456.
25 A. Mohebbi, S. Yaripour, A. S. Alavian, M. M. Daghi and N. Fattahi, *J. Food Compos. Anal.*, 2025, **138**, 107006.
26 Y. Guo, J. Wang, L. Hao, Q. Wu, C. Wang and Z. Wang, *J. Chromatogr. A*, 2021, **1649**, 462238.
27 D. N. da Silva and A. C. Pereira, *Electrochem*, 2022, **3**, 809–819.
28 Y. F. Ma, F. Yuan, X. H. Zhang, Y. L. Zhou and X. X. Zhang, *Analyst*, 2017, **142**, 3212–3218.
29 Q. N. Tran, H. J. Lee and N. Tran, *Polymers*, 2023, **15**, 1279.
30 L. C. Lin, M. Thirumavalavan, Y.-T. Wang and J.-F. Lee, *Colloids Surf., A*, 2010, **369**, 223–231.
31 X. Zhong, Z. Ren, Q. Ling and B. Hu, *Appl. Surf. Sci.*, 2022, **597**, 153621.
32 N. Huang, X. Chen, R. Krishna and D. Jiang, *Angew. Chem., Int. Ed. Engl.*, 2015, **54**, 2986–2990.
33 Z. Li, Y. Zhang, H. Xia, Y. Mu and X. Liu, *Chem. Commun.*, 2016, **52**, 6613–6616.
34 F. Li, J. L. Kan, B. J. Yao and Y. B. Dong, *Angew. Chem., Int. Ed. Engl.*, 2022, **61**, e202115044.
35 Y. Xie, L. Chen, K. Cui, Y. Zeng, X. Luo and X. Deng, *Talanta*, 2024, **279**, 126547.
36 Y. Liu, H. Zhang, D. Xie, H. Lai, Q. Qiu and X. Ma, *J. Environ. Chem. Eng.*, 2022, **10**, 108094.
37 Y. Zhao, R. Wu, H. Yu, J. Li, L. Liu, S. Wang, X. Chen and T. D. Chan, *J. Chromatogr. A*, 2020, **1610**, 460543.
38 C. Hui, C. Shen, J. Tian, L. Bao, H. Ding, C. Li, Y. Tian, X. Shi and H. J. Gao, *Nanoscale*, 2011, **3**, 701–705.
39 J. Tan, S. Namuangruk, W. Kong, N. Kungwan, J. Guo and C. Wang, *Angew. Chem., Int. Ed. Engl.*, 2016, **55**, 13979–13984.
40 Q. B. Fu, H. L. Jiang, L. Q. Qiao, X. Sun, M. L. Wang and R. S. Zhao, *J. Chromatogr. A*, 2020, **1630**, 461534.
41 Z. C. Chen, H. B. Xu, H. Y. Chen, S. C. Zhu, W. F. Huang, Y. He, M. E. Hafez, R. C. Qian and D. W. Li, *Anal. Chem.*, 2022, **94**, 14280–14289.
42 S. Bhattacharya, A. Roychowdhury, D. Das and S. Nayar, *RSC Adv.*, 2015, **5**, 89488–89497.
43 Q. Sun, B. Aguila, L. D. Earl, C. W. Abney, L. Wojtas, P. K. Thallapally and S. Ma, *Adv. Mater.*, 2018, **30**, e1705479.
44 G. Lin, C. Gao, Q. Zheng, Z. Lei, H. Geng, Z. Lin, H. Yang and Z. Cai, *Chem. Commun.*, 2017, **53**, 3649–3652.
45 M. Zhang, J. Li, C. Zhang, Z. Wu, Y. Yang, J. Li, F. Fu and Z. Lin, *J. Chromatogr. A*, 2020, **1615**, 460773.
46 Y. Du, X. Yan, Y. Chen, Y. Wu, Q. Qiu, Y. Li and D. Wu, *J. Chromatogr. A*, 2022, **1675**, 463184.
47 Z. Yan, B. Hu, Q. Li, S. Zhang, J. Pang and C. Wu, *J. Chromatogr. A*, 2019, **1584**, 33–41.
48 Z. Ma, L. Fang, L. Liu, B. Hu, S. Wang, S. Yu and X. Wang, *Sci. Total Environ.*, 2023, **901**, 166453.
49 J. Kang, S. J. Park, H. C. Park, M. A. Hossain, M. A. Kim, S. W. Son, C. M. Lim, T. W. Kim and B. H. Cho, *Appl. Biochem. Biotechnol.*, 2017, **182**, 635–652.
50 X. Guo, H. Tian, F. Yang, S. Fan, J. Zhang, J. Ma, L. Ai and Y. Zhang, *Front. Nutr.*, 2022, **9**, 879518.
51 S. Seidi, F. Mohammadi, M. Tajik, M. Baharfar, A. Mohammadi and T. Otoufat, *J. Sep. Sci.*, 2020, **43**, 2897–2904.
52 Y. Sun, J. Kuang, Y. Cheng, C. Lin, H. Zhang, M. Zhang, F. Ning and P. Hu, *J. Chromatogr. A*, 2024, **1713**, 464521.
53 J. Chen, G. Mei, X. Zhang, D. Huang, P. He and D. Xu, *Foods*, 2024, **13**, 866.
54 G. Wang, T. Zhou and Y. Lei, *RSC Adv.*, 2020, **10**, 11557–11564.
55 M. Li, W. Liu, X. Meng, S. Li, Q. Wang, Y. Guo, Y. Wu, L. Hao, X. Yang, Z. Wang, C. Wang and Q. Wu, *Food Chem.*, 2022, **395**, 133596.
56 W. Fan, D. Yang, N. Ding, P. Chen, L. Wang, G. Tao, F. Zheng and S. Ji, *Anal. Methods*, 2021, **13**, 1412–1421.
57 A. Kasperkiewicz and J. Pawliszyn, *Food Chem.*, 2021, **339**, 127815.
58 M. Liang, N. Li, H. Zhang, L. Ma and K. Wang, *RSC Adv.*, 2024, **14**, 8726–8734.
59 K. D. Lenz, K. E. Klosterman, H. Mukundan and J. Z. Kubicek-Sutherland, *Toxins*, 2021, **13**, 347.
60 Z. Sun, L. Zhao, C. Liu, Y. Zhen and J. Ma, *Chem. Eng. J.*, 2020, **381**, 122510.
61 M. Sun, S. Han, H. M. Loussala, J. Feng, C. Li, X. Ji, J. Feng and H. Sun, *Microchem. J.*, 2021, **166**, 106263.
62 J. Zhao, H. Cheng, J. Feng, T. Tang and D. Qin, *Microchem. J.*, 2024, **205**, 111241.
63 S. Li, C. Zhang, H. X. Tang, Y. Gu, A. J. Guo, K. Wang and K. Q. Lian, *J. Food Drug Anal.*, 2023, **31**, 73–84.
64 R. A. Perez, B. Albero, M. Ferriz and J. L. Tadeo, *J. Pharm. Biomed. Anal.*, 2017, **146**, 79–85.
65 W. Zheng, J. A. Park, A. M. Abd El-Aty, S. K. Kim, S. H. Cho, J. M. Choi, M. Warda, J. Wang, J. H. Shim and H. C. Shin, *Biomed. Chromatogr.*, 2018, **32**, e4145.